

Article

Intrinsic Catalytic Activity of Gold/Multi-Walled Carbon Nanotubes Composites in Squaric Acid-Iron(II/III) System

Yanxia Li ^{1,*} , Cheng Jiang ², Shengheng Lin ¹, Jiajia Lai ¹, Liyun Zheng ¹ and Pengjun Xu ^{3,*} 

¹ Department of Chemical Engineering and Materials, Ocean College, Minjiang University, Fuzhou 350108, China; lshxyy01@163.com (S.L.); 1303724217jj@gmail.com (J.L.); q971859217@gmail.com (L.Z.)

² Institute of Energy, Jiangxi Academy of Sciences, Nanchang 330096, China; jc_hyy@foxmail.com

³ Faculty of Clothing and Design, Minjiang University, Fuzhou 350108, China

* Correspondence: yxli09@163.com (Y.L.); xupj@mju.edu.cn (P.X.); Tel: +86-13665034805 (Y.L.); +86-18649807883 (P.X.)

Received: 20 March 2018; Accepted: 30 April 2018; Published: 2 May 2018



Abstract: In this paper, gold/multi-walled carbon nanotube (Au/MWCNTs) composites were prepared via in situ reductions. The synthesized materials could effectively catalyze the system of square acid (SQA)-iron(II/III) to produce a significant color reaction. By designing the orthogonal test of three-factor and three-level, the three factors of sodium formate solution concentration, ultrasonic time and synthesis reaction time were optimized in the process of Au/MWCNTs preparation. Results showed that the Au/MWCNTs had the best catalytic activity under the conditions of sodium formate solution concentration of 400 mmol/L, ultrasonic for 30 min and reaction for 4 h. In a subsequent comparison with H₂O₂, it found that the catalytic performance of 1 mg of Au/MWCNTs composite was equivalent to that of H₂O₂ with the concentration of 0.28 mmol/L. It demonstrated that the prepared Au/MWCNTs composites had good catalytic activity, stable color and low background noise, indicating a good prospect in various fields including that of catalytic reaction, sensing analysis, and nanomaterials labeling.

Keywords: Au/MWCNTs composites; catalytic activity; square acid-iron(II/III) system

1. Introduction

Hybrids with catalytic activity based on different nanomaterials, such as iron oxide [1], metal-organic frameworks [2], grapheme [3], carbon nanotubes (CNTs) [4] have been successfully applied to various fields. Among these materials, CNTs have been extensively employed for synthesis of hybrid materials in sensing and catalysis due to their electrical conductivity, high chemical stability, unusual conjugated structure, and significant mechanical strength [5–7]. Cui et al. developed helical CNTs by employing the hydrothermal/hydrogen reduction method, involving a large specific surface area and high catalytic activity [8]. As the catalyst support, extensive efforts have been made in the past several decades. There are many applications of CNTs which are often hybridized by organic polymer [9], graphene oxide [10], metallic oxide [11,12], metal (Ni, Pt, Au) [13,14], along with other materials. These nanocomposites express special advantages in the high surface area to volume ratios, which provide a unique opportunity for catalyst supports, enhancing the catalyst longevity and sensitivity [15]. To date, Au/CNTs hybrids have been extensively studied and have known to become well-researched materials [6,16]. Technically, Au nanoparticles can easily be prepared onto CNTs by direct chemical reduction [17,18]. Due to its simple preparation, catalytic activity is easy to mark, and Au/CNTs hybrids have been mainly used in sensing analysis [19,20].

The catalytic activity of Au/CNTs hybrids has been applied in colorimetric assays for real-time naked-eye detection, as the Au/CNTs hybrids can efficiently catalyze the oxidation of 3,3',5,5'-tetramethylbenzidine (TMB) to yield a blue colored product in the presence of H₂O₂ [4,21]. However, this process of catalytic chromogenic reaction needs H₂O₂ to participate in the reaction, and H₂SO₄ to stop the reaction. Furthermore, the color produced by the system is influenced by the acidity or alkalinity of the solution. With the increase of acidity, the color of the solution eventually turns yellow. Fresh H₂O₂ and oxygen-free are the keys to the color reaction.

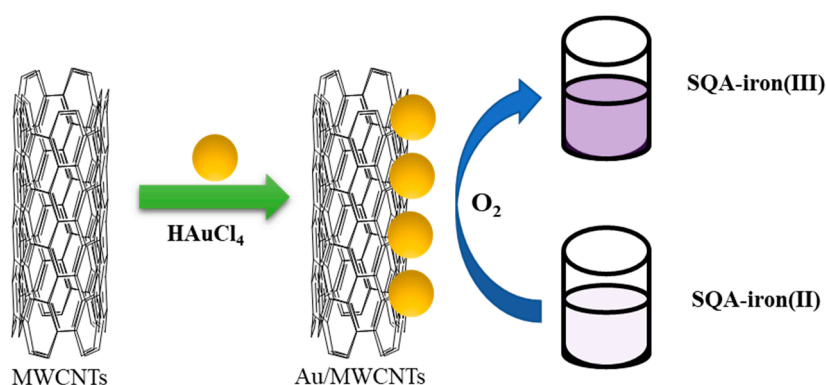
In recent years, square acid(SQA)-iron(II/III) chelate has been successfully used to colorimetric sensors [22,23]. SQA, a two-dimensional planar structure of squarate C₄O₄ units linked by protons in a layered sheet, is a moderately strong acid ($K_{a1} \approx 0.4$, $K_{a2} = 1.58 \times 10^{-3}$ M). When iron(II) is oxidized to iron(III), SQA can rapidly react with iron(III) in a very short time, forming SQA-iron(III) chelate which can cause a purple solution [24]. The facile ability of iron to gain and lose electrons permits its participation in a wide variety of oxidation-reduction reactions. Lai et al. constructed a simple and feasible colorimetric immunoassay with signal amplification, for sensitive determination of prostate-specific antigen at an ultralow concentration by glucose oxidase stimulating in situ formation of SQA-iron(III) chelate [25]. Due to its rapid, stable, and sensitive properties, the system of SQA-iron(II/III) chelate has potential applications in the field of catalysis and chromogenic sensing.

Herein, we prepared gold/multi-walled carbon nanotubes (Au/MWCNTs) composites by one-step in situ preparation. Orthogonal test of three-factor and three-level in the process of preparation further improved the catalytic activity of Au/MWCNTs composites, which can effectively catalyze the oxidation of Iron(II) to Iron(III) causing a purple color chelated with SQA in the absence of H₂O₂. The intrinsic catalytic activity of Au/MWCNTs composites combined with SQA-iron(II/III) chelate has a good prospect in the fields of catalytic reaction, sensing analysis, nano-materials labeling, and so on.

2. Results and Discussion

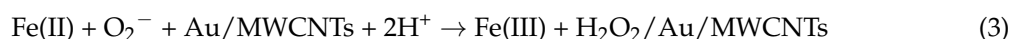
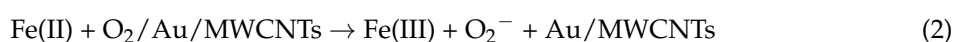
2.1. Principle of Catalytic Activity by SQA-Iron(II/III) Chelate

The one-step in situ preparation of Au/MWCNTs composites was performed with simple operations under mild conditions. The mechanism and the effect of the high intensity ultrasonic processing were to accelerate the acid etching of the MWCNTs surface by H₂AuCl₄, which introduces structural defects that allows the attachment of Au³⁺ ions. As commonly known, the Au/CNTs catalyze the oxidation of TMB by H₂O₂ to develop a blue color in an aqueous solution. Therefore, Au/CNTs composites have been applied extensively in catalysis and sensors. However, the blue color produced by the catalytic reaction is not very stable and the catalytic reaction requires an acid solution to stop the reaction. The color reaction of SQA-iron(II/III) chelate by catalysis shows high sensitivity and stability with low background signal. In our previous study, we constructed glucose visible spectral analysis based on the chelating system of SQA-iron(II/III), which showed high sensitivity and good stability for 8 h [26]. Lai et al. reported a kind of ultrasensitive colorimetric immunoassay accompanying cascade reaction for enzymatic formation of SQA-iron(II/III) chelate. The sensitivity displayed to be 3–5 orders of magnitude better than those of most commercialized human prostate-specific antigen(PSA) enzyme-linked immunosorbent assay (ELISA) kits [25]. However, compared to TMB color reaction system, SQA-iron(III) chelate has not been widely used. It may be due to the fact that square acid is not a commonly used reagent. Along with adding depth to the research, SQA-iron(II/III) chelate system will be used in various ways across many fields, particularly in sensors. Therefore, we employ the use of the catalytic activity of Au/MWCNTs composites to catalyze SQA-iron(II/III) chelate and develop a clear purple color in aqueous solution under mild reaction conditions. Scheme 1 displays the catalytic activity of Au/MWCNTs composites under the SQA-iron(II/III) system.



Scheme 1. The catalytic activity of Au/MWCNTs composites under the SQA-iron(II/III) system.

The possible reaction mechanism is that the Au/MWCNTs catalyzes Fe(II) oxidized into Fe(III) by dissolved O_2 in an aqueous solution and oxygen in the air. Fe(II) oxidation is a critical process in the present catalytic reaction. The most accepted mechanisms of Fe(II) oxidation by dissolved O_2 are shown as below [27]:



The chelation reaction between Fe(III) and SQA can be completed within 1 min. Therefore, reactions 2 and/or 4 are the rate determining steps. The Au atoms of Au/MWCNTs can induce O_2 dissociation [28], thus speeding up the step of the reaction 2. At the same time, the larger surface area of Au/MWCNTs increases the number of combined O_2 .

The saturation concentration of dissolved oxygen in pure water is about 8 mg/L at room temperature and atmospheric pressure. According to the possible reaction mechanism, oxygen is a kind of initiator, and the prepared Au/MWCNTs can speed up the step of the reaction 2. All the reaction of step 2,3,4 and 5 can oxidize Fe^{2+} to Fe^{3+} . Although there is a low oxygen concentration in the aqueous solution, oxygen in the air is enough to oxidize Fe^{2+} . To identify the role of oxygen in the catalytic reaction system, control of N_2 deoxygenation for 10 min before the catalytic reaction was carried out at air (N_2 deoxygenation) and nitrogen (absence of O_2) atmosphere, respectively. As shown in Figure 1, the absorbance of catalytic reaction in the presence of oxygen is higher than N_2 deoxygenation and absence of O_2 , which indicated the role of dissolved oxygen and oxygen in the air in the catalytic reaction. The oxygen in the air plays a key role in the process of reaction.

The elimination of H_2O_2 , as an intermediate product, was identified by catalase. When catalase (1.0 mmol/L) was added in the catalytic reaction, as shown in Figure 1, the absorbance of catalytic reaction in the presence of catalase is lower than in the absence of catalase, which indicated elimination of H_2O_2 in the catalytic reaction. However, there is still background color which may be due to the instability of Fe(II), such as illumination, oxygen in the air, dissolved oxygen in the reaction solution. Therefore, it is a complex reaction process. A stable result can be obtained at the normal temperature and atmospheric pressure. O_2 and eliminating H_2O_2 can affect the catalytic reaction.

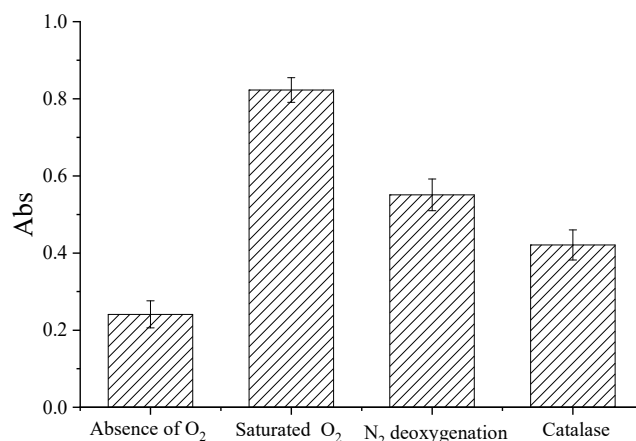


Figure 1. The catalytic reaction in the presence or absence of oxygen.

2.2. Characteristics of Au/MWCNTs Composites

The TEM morphologies of MWCNTs and Au/MWCNTs composites are shown in Figure 2. Figure 2a shows that the average diameter of the MWCNTs is about 30 nm with uniform nanotubes. Figure 2b shows that the Au nanoparticles (NPs) are securely attached to the MWCNTs surface and can be clearly distinguished from MWCNTs. The average Au NPs size was ~10 nm. Usually, nanoparticles of smaller size show a greater catalytic activity due to the large surface to volume ratio for interaction with substrates [29,30]. As Ahmed et al. reported [21], the size of Au NPs depends on the concentration of sodium formate during synthesis. At the same time, SEM Micrographs of Au NPs as control (c), Au/MWCNTs composites (d) showed Au NPs with ~10 nm size and Au NPs on the surface of MWCNTs.

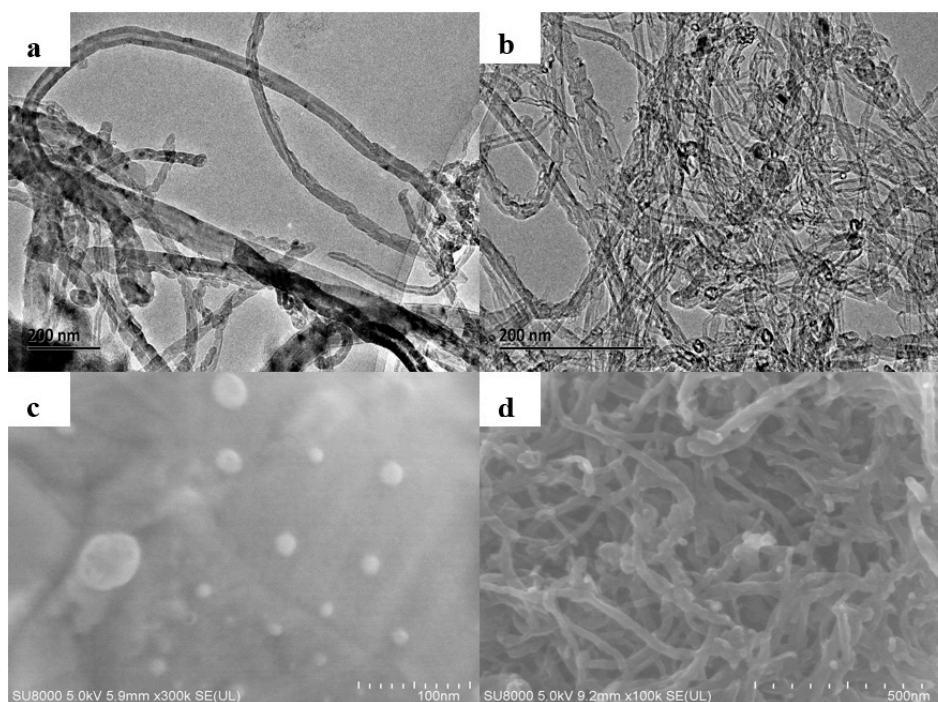


Figure 2. TEM Micrographs of the MWCNTs (a), Au/MWCNTs composites (b) and SEM micrographs of Au NPs (c), Au/MWCNTs composites (d).

The structure of Au/MWCNTs is also characterized by X-ray diffraction (XRD). As shown in Figure 3, the peak at a low angle ($2\theta = 26.05^\circ$) of MWCNTs is indexed to the (002) plane of graphitic crystallinity of the MWCNTs [31]. The peaks at 38.18, 44.48, 64.68 and 77.68 are ascribed to (111), (200), (220) and (311) reflections of Au face-centered cubic crystallographic structure (JCPDS card No. 65-2870). All of the patterns illustrate that Au has been successfully loaded onto the MWCNTs.

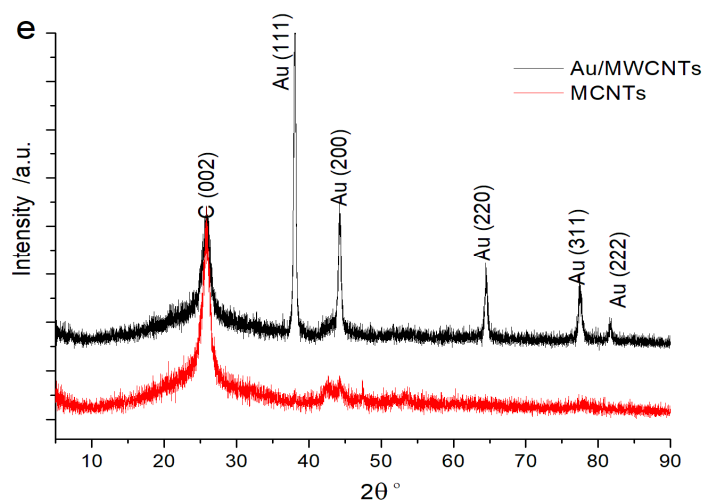


Figure 3. XRD spectra of Au/MWCNTs (black), MWCNTs (red).

2.3. Optimized Synthesis of Au/MWCNTs Composites by Orthogonal Design

In order to improve the catalytic activity of Au/MWCNTs composites under the SQA-iron(II/III) system, three influential factors in the synthesis process were investigated, which included ultrasonic time, sodium formate concentration and reaction time. Orthogonal test of three factors and three levels was carried out to optimize the reaction conditions (Table 1). The synthesized Au/MWCNTs composites under the different conditions further catalyzed the SQA-iron(II/III) system to develop a purple color recorded by the absorbance measurement at 537 nm (Table 2). As shown in Table 2, the catalytic effect of the synthesized materials was quite different under the different synthetic conditions. Under the condition of No. 5, the maximum absorbance of 0.574 ± 0.024 was observed, which proved to be the best catalytic effect. Therefore, 30 min of ultrasonic time, 400 mmol/L of sodium formate concentration and 4 h of reaction time were selected as the optimized synthesis conditions.

Table 1. Orthogonal design of three factors and three levels.

Levels	Ultrasonic Time (min)	Sodium Formate Concentration (mmol/L)	Reaction Time (h)
1	5	200	1
2	30	400	2
3	60	600	4

Table 2. Catalytic activity of Au/MWCNTs composites with the SQA-iron(II/III) system under orthogonal design of three factors and three levels.

No.	Ultrasonic Time (min)	Sodium Formate Concentration (mmol/L)	Reaction Time (h)	Absorbance
1	5	200	1	0.386 ± 0.017
2	30	200	2	0.464 ± 0.033
3	60	200	4	0.438 ± 0.028
4	5	400	2	0.358 ± 0.019
5	30	400	4	0.574 ± 0.024
6	60	400	1	0.509 ± 0.030
7	5	600	4	0.439 ± 0.021
8	30	600	1	0.433 ± 0.032
9	60	600	2	0.464 ± 0.020

2.4. Performance of Catalytic Activity

As commonly observed, H_2O_2 can catalytically oxidize iron(II) to iron(III), which can rapidly (<1 min) coordinate with the SQA. Formation of the iron-squarate complex to generate the purple color, which has a direct correlation with the iron(II/III) concentration. Experiments show that the Au/MWCNTs composites with catalytic activity can replace H_2O_2 in the chromogenic reaction of SQA-iron(II/III) system. To confirm the unique catalytic activity of Au/MWCNTs composites, UV-Vis spectra of SQA-iron(II/III) system catalyzed by Au/MWCNTs (a), MWCNTs (b), Au NPs (c), H_2O for blank control (d) were measured (Figure 4). As shown in Figure 4, SQA-iron(II) system was stable with no color (Figure 4d); Au NPs (Similar to the Au/MWCNTs synthesis method in the absent of MWCNTs) also showed no catalytic activity. However, MWCNTs had a slight catalytic activity in SQA-iron(II) system. This phenomenon may be due to the large specific surface area of MWCNTs. On the other hand, when Au and MWCNTs were hybridized, there were significant color changes, which had a visible absorption at 537 nm. This suggests that the hybridization of Au NPs changes the surface structure of MWCNTs. The Au/MWCNTs composites could catalyze the formation of SQA-iron(III) chelate from the SQA-iron(II) system. The proposed mechanism is that gold nanocrystals absorbed on MWCNTs are formed during the synthesis process which has exceptional properties in oxidation catalysis [31].

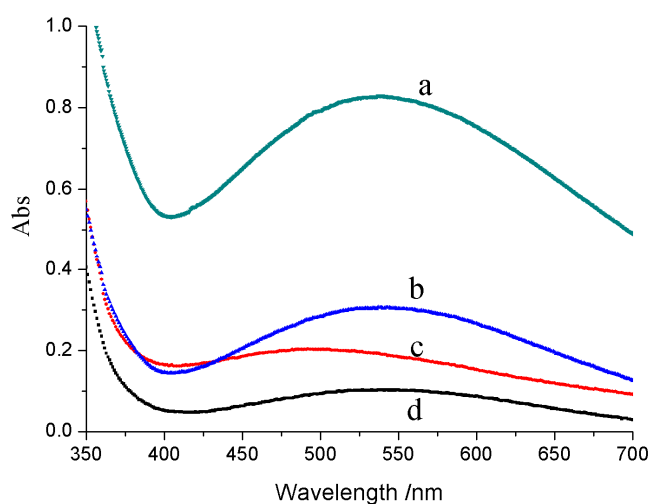


Figure 4. UV-Vis spectra of SQA-iron(II/III) system catalyzed by Au/MWCNTs (a); MWCNTs (b); Au NPs (c); H_2O for blank control (d).

2.5. Optimization of SQA Concentration

To improve the sensitivity of chromogenic reaction, it is very important to control the reactant concentrations of SQA and iron(II). The optimization of the conditions was carried out through changing the concentration of SQA when the concentration of ferrous sulfate was set to 80 mmol/L. Figure 5 shows the absorbance curve (A) and photograph (B) after the reactions at different SQA concentration with iron(II) were catalyzed by Au/MWCNTs. From the absorbance curve, the chromogenic reaction exhibited a sensitive color change. As the SQA concentration increased, the absorbance increased rapidly and tended to be stable at 80 mmol/L of SQA concentration with the maximum absorbance of 0.830, which indicated that 80 mmol/L was the optimization of SQA concentration.

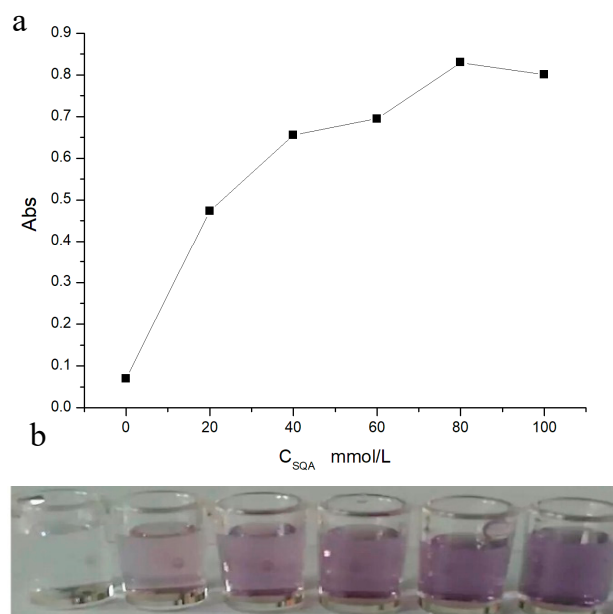


Figure 5. Absorbance curve at 537 nm (a) and photograph (b) after the reactions at different SQA concentration with iron(II) catalyzed by Au/MWCNTs. From left to right: 0, 20, 40, 60, 80 and 100 mmol/L; The iron(II) concentration: 80 mmol/L.

2.6. The Conversion Rate of Iron(II)

As per the optimization of SQA concentration, 80 mmol/L of SQA concentration can be achieved the best color when iron(II) concentration is 80 mmol/L. To investigate the yield of the chelation reaction, iron(III) was directly chelated with square acid (80 mmol/L) in the absence of Au/MWCNTs and iron(II). As shown in Figure 6, the absorbance of chelate products increased with increasing of iron(III) concentration and tended to be stable at 40 mmol/L of iron(III) concentration with the maximum absorbance. This observation suggests that the chelating reaction between SQA and iron(III) is completed with the stoichiometric ratio of 2:1. Therefore, 80 mmol/L of iron(II) in the catalytic reaction was the overdose. Overdose iron(II) was beneficial to increase the catalytic reaction rate and to produce more sensitive coloration. The conversion rate of iron(II) to iron(III) is at least 50%. Excess iron(III) converted by iron(II) cannot further deepen the color.

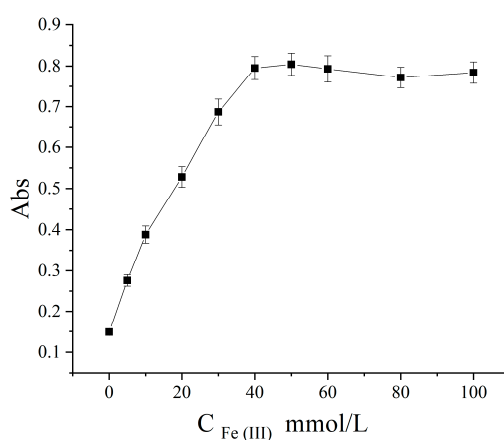


Figure 6. Absorbance curve changed with iron(III) concentration. The SQA concentration: 80 mmol/L.

2.7. Effects of pH in the Catalytic Process

Solution pH is one of the most important factors affecting the oxidation assays of Fe(II) to Fe(III). To evaluate the effects of pH values in the catalytic process, a series of experiments were carried out in a series of Fe(II) solutions with different pH ranging from 4.0 to 10.0 (Figure 7). As commonly known, Fe(II) can be slowly oxidized to Fe(III) by dissolved O₂ in an acid solution. From the result, it can be found that with increasing pH, the value of absorbance after the catalytic reaction was stable under acidic conditions, and then gradually decrease with the increase of pH in the alkaline environment. This phenomenon may be due to Fe(II) being successfully oxidized to Fe(III) by Au/MWCNT catalysis. Therefore, the acid and neutral condition do not affect the color change of the chelating products. Fe(III) can be easily precipitated in an alkaline solution, causing absorbance reduction of chelating products. Therefore, 7.0 was selected as the optimized pH solution. At the same time, the effect of pH showed alkaline environment inhibiting the catalytic reaction. This phenomenon also supports the reaction mechanism due to the formation of hydroxyl ion in the process of catalytic reaction.

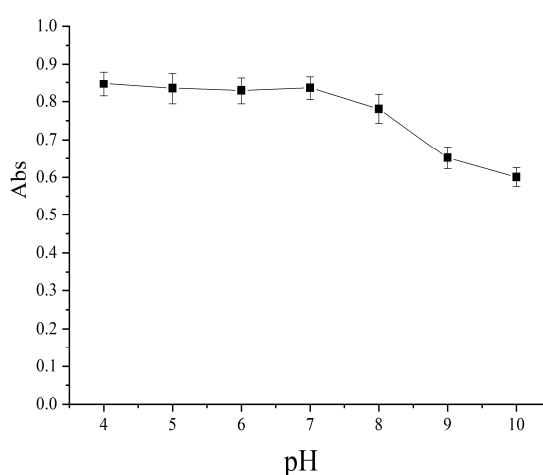


Figure 7. Absorbance curve after catalytic reaction changed with pH of the SQA-iron(II) solution.

2.8. Kinetics of Catalytic Reaction and Stability of Chelating Product

To gain further insight into the catalytic reaction mechanism, the rate of catalytic reaction and stability of chelating product were studied. The experiments were performed over a time course of the catalytic reaction by Au/MWCNTs. Figure 8a shows that the curve of absorbance changed with the time of the catalytic reaction. It is apparent that the catalytic reaction proceeded rapidly and was completed within 30 min. This phenomenon indicates that it needs 30 min to completely oxidize iron(II) to iron(III). Furthermore, it shows good stability within 24 h. Figure 8b shows the SQA-iron(II) solution in the absence of Au/MWCNTs under the room temperature and atmospheric pressure. Fe(II) can be oxidized into Fe(III) by dissolved O₂ in an aqueous solution and oxygen in the air. As we can see from Figure 8b, the color of the solution also deepens with time. However, the changes in absorbency were not obvious. This phenomenon indicates that Au/MWCNTs plays a catalytic role in the SQA-iron(II/III) system. The rapid catalytic reaction and good stability are beneficial to further the application of Au/MWCNTs-SQA-iron(II/III). For example, Au/MWCNTs can be used as a biomarker as it is rich in Au on the surface of MWCNTs, which is easy to bond with thiol by Au-S. Moreover, SQA-iron(II/III) system, as a chromogenic agent, has many advantages, such as mild reaction conditions, easy operation, high sensitivity, good stability and so on.

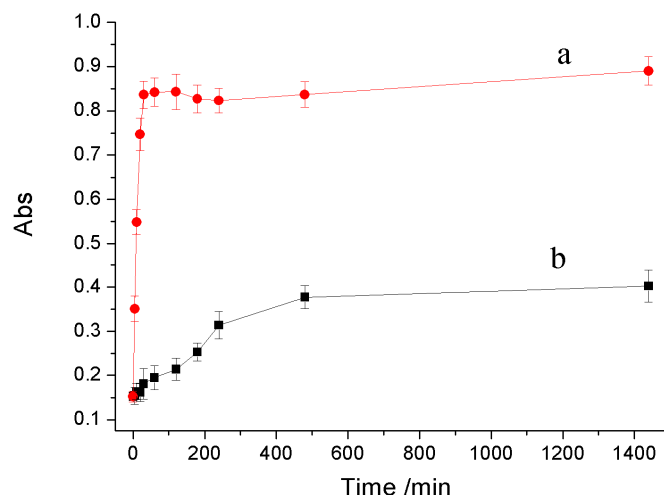


Figure 8. Kinetics of catalytic reaction and stability of chelating product. Catalytic reaction in the present (a) and absent (b) of Au/MWCNTs.

2.9. Catalytic Activity Compared with H_2O_2

To calculate and evaluate the catalytic activity of Au/MWCNTs, a comparison was made between Au/MWCNTs and H_2O_2 . It is reported that H_2O_2 has highly efficient catalysis on the SQA-iron(III) chelate because H_2O_2 (as a strong oxidizer) can oxidize iron(II) to iron(III) [32,33]. Therefore, upon addition of H_2O_2 into the SQA-iron(II) system under the same condition of Au/MWCNTs catalytic system, the absorbance at 537 nm increased with the increase in H_2O_2 concentrations. As shown in Figure 9, a positive linear relationship was obtained between the SQA-iron(II) system and H_2O_2 solutions with various final concentrations. 1.0 mg of Au/MWCNTs was equivalent to 0.28 mmol/L of H_2O_2 by absorbance calculation which indicated a high catalytic activity of the synthesized Au/MWCNTs.

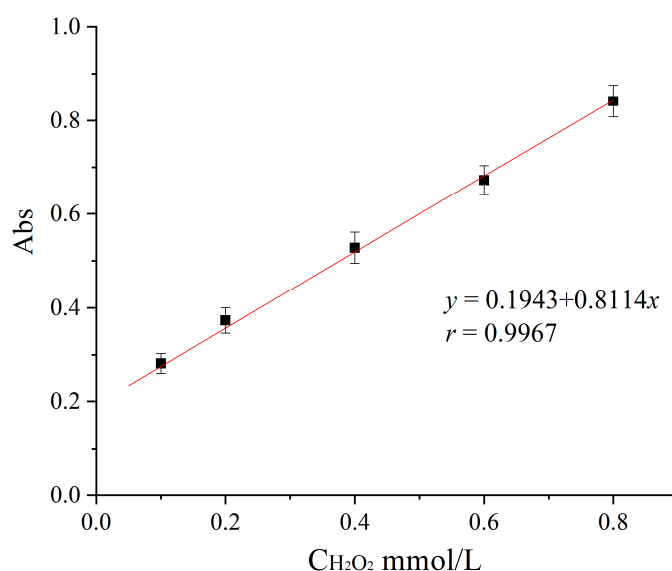


Figure 9. Linear plots of the SQA-iron(II/III) system toward H_2O_2 standards with various final concentrations.

3. Materials and Methods

3.1. Materials

MWCNTs (diameter < 20 nm) were purchased from Nanjing XFNANO Technology Co., Ltd. (Nanjing, China). The MWCNTs were purified through refluxing in nitric acid and recollected for further application. 3,3',5,5'-tetramethylbenzidine (TMB), sodium formate were purchased from Aladdin reagent (Shanghai) Co., Ltd. (Shanghai, China). Square acid (SQA) was purchased from Alfa Aesar Chemical Co. Ltd. (Shanghai, China) Ferrous sulfate (FeSO_4), 30% H_2O_2 , gold chloride tetrahydrate ($\text{HAuCl}_4 \cdot 4\text{H}_2\text{O}$), were all analytical grade received from Xinyuhua (Fuzhou, China). All the reagents were used without further purification. Double-distilled water was used throughout the study.

3.2. Apparatus

The morphologies and structures of the magnetic nanomaterials were examined using transmission electron microscope (TEM, Tecnai F30 G2 S-TWIN 300 KV, FEI, Hillsboro, OR, USA) and field emission scanning electron microscope (SEM; SU8000, Hitachi, Japan). The samples for TEM were dispersed in ethanol and a drop of the dispersion was spread on amorphous carbon-coated 200 mesh copper grids, followed by drying at the ambient temperature. A UV-vis spectrophotometer (UV-2450, Shimadzu, Japan) was used to determine the absorbance of the color-reaction. All experiments were performed under a dry nitrogen atmosphere, at the room temperature.

3.3. Preparation of Au/MWCNTs Composites

The preparation process of Au/MWCNTs composites was optimized on the basis of the literature reported [21]. At first, 2 mg MWCNTs was added to 1 mL 1% HAuCl_4 aqueous solution with ultrasonic vibration for 30 min, then mixed with 2 mL 400 mmol/L sodium formate solution and gently shaken for 4 h at the room temperature. Finally, Au/MWCNTs composites were obtained by centrifugation at 4000 rpm for 5 min and thoroughly washed for 6 times with water and dispersed in 1 mL water.

3.4. Catalytic Activity Assay

Initially, 70 μL of 80 mmol/L FeSO_4 was added into 100 μL of the above-prepared Au/MWCNTs solution. Then, 70 μL of 80 mmol/L SQA was quickly injected into the resulting solution (40 mmol/L SQA was used in orthogonal design and performance of catalytic activity). After interaction for 30 min, the absorbance was recorded at $\lambda = 537$ nm by UV-vis spectrophotometer.

4. Conclusions

In summary, we introduced a straightforward method for the preparation of Au/MWCNTs composites via the one-step in situ reductions of Au on MWCNTs. By designing the orthogonal test in the synthesis process, Au/MWCNTs composites with high catalytic activity were obtained through the highly sensitive SQA-iron(II) reaction. It was found that the catalytic performance of 1 mg Au/MWCNTs composite was equivalent to that of H_2O_2 at the concentration of 0.39 mmol/L. The Au/MWCNTs-SQA-Fe(II/III) system showed mild reaction conditions, easy operation, high sensitivity and good stability. The catalytic reaction system of Au/MWCNTs-SQA-iron(II/III) has a good prospect in various fields, particularly in catalytic reaction, sensing analysis, and nano-materials labeling.

Author Contributions: Yanxia Li and Pengjun Xu designed the experiments. Shengheng Lin, Jiajia Lai and Liyun Zheng performed the experiments. Cheng Jiang analyzed the data. Yanxia Li wrote the paper.

Acknowledgments: This work was financially supported by NSFC (21405075, 51403098), Industrial technology key project of Fujian Province (2014H0040), Fujian province natural science foundation (2016J05040, 2017J01418), Fujian provincial youth natural fund key project (JZ160468), The plan of college youth outstanding research talents in Fujian Province (2015), and program for new century excellent talents of university in Fujian Province (2017).

Conflicts of Interest: The authors declare no conflict of interest.

References

1. Li, J.; Cai, J.; Jia, H.; Zhang, L.; Lei, Y.; He, W. Formation of iron oxide/Pd hybrid nanostructures with enhanced peroxidase-like activity and catalytic reduction of 4-nitrophenol. *J. Environ. Sci. Health C* **2017**, *35*, 159–172. [[CrossRef](#)] [[PubMed](#)]
2. Tan, H.; Li, Q.; Zhou, Z.; Ma, C.; Song, Y.; Xu, F.; Wang, L. A sensitive fluorescent assay for thiamine based on metal-organic frameworks with intrinsic peroxidase-like activity. *Anal. Chim. Acta* **2015**, *856*, 90–95. [[CrossRef](#)] [[PubMed](#)]
3. Ahmed, S.R.; Takemeura, K.; Li, T.C.; Kitamoto, N.; Tanaka, T.; Suzuki, T.; Park, E.Y. Size-controlled preparation of peroxidase-like graphene-gold nanoparticle hybrids for the visible detection of norovirus-like particles. *Biosensors Bioelectron.* **2017**, *87*, 558–565. [[CrossRef](#)] [[PubMed](#)]
4. Qian, J.; Yang, X.; Yang, Z.; Zhu, G.; Mao, H.; Wang, K. Multiwalled carbon nanotube@reduced graphene oxide nanoribbon heterostructure: Synthesis, intrinsic peroxidase-like catalytic activity, and its application in colorimetric biosensing. *J. Mater. Chem. B* **2015**, *3*, 1624–1632. [[CrossRef](#)]
5. Hsu, C.W.; Lin, Z.Y.; Chan, T.Y.; Chiu, T.C.; Hu, C.C. Oxidized multiwalled carbon nanotubes decorated with silver nanoparticles for fluorometric detection of dimethoate. *Food Chem.* **2017**, *224*, 353–358. [[CrossRef](#)] [[PubMed](#)]
6. Xiao, J.; Pan, X.; Guo, S.; Ren, P.; Bao, X. Towards fundamentals of confined catalysis in carbon nanotubes. *J. Am. Chem. Soc.* **2015**, *137*, 477–482. [[CrossRef](#)] [[PubMed](#)]
7. Melchionna, M.; Marchesan, S.; Prato, M.; Fornasiero, P. Cheminform abstract: Carbon nanotubes and catalysis: The many facets of a successful marriage. *Catal. Sci. Technol.* **2015**, *5*, 3859–3875. [[CrossRef](#)]
8. Cui, R.; Han, Z.; Zhu, J.J. Helical carbon nanotubes: Intrinsic peroxidase catalytic activity and its application for biocatalysis and biosensing. *Chemistry* **2011**, *17*, 9377–9384. [[CrossRef](#)] [[PubMed](#)]
9. Liu, K.; Li, C.; Zhang, X.; Hua, W.; Yang, D.; Hu, J.; Yue, Y.; Gao, Z. Poly(styrene sulfonic acid)-grafted carbon nanotube as a stable protonic acid catalyst. *Catal. Commun.* **2010**, *12*, 217–221. [[CrossRef](#)]
10. Nahorny, S.; Zanin, H.; Christino, V.A.; Marciano, F.R.; Lobo, A.O.; Soares, L.E.S. Multi-walled carbon nanotubes/graphene oxide hybrid and nanohydroxyapatite composite: A novel coating to prevent dentin erosion. *Mat. Sci. Eng. C* **2017**, *79*, 199–208. [[CrossRef](#)] [[PubMed](#)]
11. Qu, Z.; Miao, L.; Wang, H.; Fu, Q. Highly dispersed Fe₂O₃ on carbon nanotubes for low-temperature selective catalytic reduction of NO with NH₃. *Chem. Commun.* **2015**, *51*, 956–958. [[CrossRef](#)] [[PubMed](#)]
12. Fan, G.; Wang, H.; Xiang, X.; Li, F. Co–Al mixed metal oxides/carbon nanotubes nanocomposite prepared via a precursor route and enhanced catalytic property. *J. Solid State Chem.* **2013**, *197*, 14–22. [[CrossRef](#)]
13. Shen, Y.; Lua, A.C. Synthesis of Ni and Ni–Cu supported on carbon nanotubes for hydrogen and carbon production by catalytic decomposition of methane. *Appl. Catal. B Environ.* **2015**, *164*, 61–69. [[CrossRef](#)]
14. Aslan, E.; Akin, I.; Patir, I.H. Enhanced hydrogen evolution catalysis based on Cu nanoparticles deposited on carbon nanotubes at the liquid/liquid interface. *Chemcatchem* **2016**, *8*, 719–723. [[CrossRef](#)]
15. Huff, C.; Dushatinski, T.; Abdel-Fattah, T.M. Gold nanoparticle/multi-walled carbon nanotube composite as novel catalyst for hydrogen evolution reactions. *Int. J. Hydrog. Energy* **2017**, *42*, 18985–18990. [[CrossRef](#)]
16. Alves, L.; Ballesteros, B.; Boronat, M.; Cabrero-Antonino, J.R.; Concepción, P.; Corma, A.; Correa-Duarte, M.A. Synthesis and stabilization of subnanometric gold oxide nanoparticles on multiwalled carbon nanotubes and their catalytic activity. *J. Am. Chem. Soc.* **2011**, *133*, 10251–10261. [[CrossRef](#)] [[PubMed](#)]
17. Cegłowski, M.; Pelech, I.; Schroeder, G. Functionalization of gold-coated carbon nanotubes with self-assembled monolayers of thiolates. *J. Mater. Sci.* **2012**, *47*, 3463–3467. [[CrossRef](#)]
18. Alexeyeva, N.; Matisen, L.; Saar, A.; Laaksonen, P.; Kontturi, K.; Tammeveski, K. Kinetics of oxygen reduction on gold nanoparticle/multi-walled carbon nanotube hybrid electrodes in acid media. *J. Electroanal. Chem.* **2010**, *642*, 6–12. [[CrossRef](#)]
19. Madhumati, R.; Mitali, P.; Rigved, E.; Yeohung, Y.; Vasselin, S.; Mark, S.; William, R.H.; Moni, K.D.; Prashant, N.K. Gold-coated carbon nanotube electrode arrays: Immunosensors for impedimetric detection of bone biomarkers. *Biosens. Bioelectron.* **2016**, *77*, 580–588.

20. Guo, W.; Zhang, A.; Zhang, X.; Huang, C.; Yang, D.; Jia, N. Multiwalled carbon nanotubes/gold nanocomposites-based electrochemiluminescent sensor for sensitive determination of bisphenol A. *Anal. Bioanal. Chem.* **2016**, *408*, 7173–7180. [[CrossRef](#)] [[PubMed](#)]
21. Ahmed, S.R.; Kim, J.; Suzuki, T.; Lee, J.; Park, E.Y. Enhanced catalytic activity of gold nanoparticle-carbon nanotube hybrids for influenza virus detection. *Biosensors Bioelectron.* **2016**, *85*, 503–508. [[CrossRef](#)] [[PubMed](#)]
22. Chen, H.; Fang, A.; He, L.; Zhang, Y.; Yao, S. Sensitive fluorescent detection of H₂O₂ and glucose in human serum based on inner filter effect of squaric acid-iron(III) on the fluorescence of upconversion nanoparticle. *Talanta* **2017**, *164*, 580–587. [[CrossRef](#)] [[PubMed](#)]
23. Kiskin, M.A.; Shvedenkov, Y.G.; Ikorskii, V.N.; Romanenko, G.V.; Ovcharenko, V.I. Molecular magnet based on the Fe II, III complex with squaric acid. *Russ. Chem. Bull.* **2003**, *52*, 265–266. [[CrossRef](#)]
24. Sisley, M.J.; Jordan, R.B. Kinetic and equilibrium studies of complexes of aqueous iron (III) and squaric acid. *Inorg. Chem.* **2002**, *30*, 2190–2195. [[CrossRef](#)]
25. Lai, W.; Tang, D.; Zhuang, J.; Chen, G.; Yang, H. Magnetic bead-based enzyme-chromogenic substrate system for ultrasensitive colorimetric immunoassay accompanying cascade reaction for enzymatic formation of squaric acid-iron (III) chelate. *Anal. Chem.* **2014**, *86*, 5061–5068. [[CrossRef](#)] [[PubMed](#)]
26. Li, Y.; Chen, Y.T.; Huang, L.; Wang, X. Spectral analysis for trace glucose measurement based on the chelating system of Fe³⁺-squaric acid. *Chin. J. Anal. Lab.* **2017**, *9*, 1019–1022.
27. Sugimori, H.; Kanzaki, Y.; Yokota, K.; Murakami, T. Nonlinear dependence of the oxidation rate of Fe (II) on dissolved oxygen under low-O₂ conditions in aqueous solutions. *J. Miner. Petrol. Sci.* **2011**, *106*, 142–152. [[CrossRef](#)]
28. Das, T.; Ghosh, P.; Shanavas, M.S.; Maity, A.; Mondal, S.; Purkayastha, P. Protein-templated gold nanoclusters: Size dependent inversion of fluorescence emission in the presence of molecular oxygen. *Nanoscale* **2012**, *4*, 6018–6024. [[CrossRef](#)] [[PubMed](#)]
29. Peng, Y.; Wang, Z.; Liu, W.; Zhang, H.; Zuo, W.; Tang, H.; Chen, F.; Wang, B. Size- and shape-dependent peroxidase-like catalytic activity of MnFe₂O₄ nanoparticles and their applications in highly efficient colorimetric detection of target cancer cells. *Dalton Trans.* **2015**, *44*, 12871–12877. [[CrossRef](#)] [[PubMed](#)]
30. Herzing, A.A.; Kiely, C.J.; Carley, A.F.; Landon, P.; Hutchings, G.J. Identification of active gold nanoclusters on iron oxide supports for CO oxidation. *Science* **2008**, *321*, 1331–1335. [[CrossRef](#)] [[PubMed](#)]
31. Li, C.; Su, Y.; Lv, X.; Xia, H.; Wang, Y. Electrochemical acetylene sensor based on Au/MWCNTs. *Sensors Actuators B Chem.* **2010**, *149*, 427–431. [[CrossRef](#)]
32. Matsubayashi, M.; Matsubayashi, M.; Morita, M. Decoloration reaction of peroxidase-H₂O₂ system to the tolerance for hydrogen peroxide. *Fiber* **2015**, *71*, 250–256. [[CrossRef](#)]
33. Yang, L.; Liu, X.; Lu, Q.; Huang, N.; Liu, M.; Zhang, Y.; Yao, S. Catalytic and peroxidase-like activity of carbon based-AuPd bimetallic nanocomposite produced using carbon dots as the reductant. *Anal. Chim. Acta* **2016**, *930*, 23–30. [[CrossRef](#)] [[PubMed](#)]

